Automatic discrimination of underwater acoustic signals generated by teleseismic P-waves: A probabilistic approach

Alexey Sukhovich,[1] Jean-Olivier Irisson,[2,3] Frederik J. Simons,[4] Anthony Ogé,[1] Yann Hello,[1] Anne Deschamps,[5] and Guust Nolet[5]

Received 17 June 2011; revised 17 August 2011; accepted 18 August 2011; published 30 September 2011.

[1] We propose a new probabilistic scheme for the automatic recognition of underwater acoustic signals generated by teleseismic P-waves recorded by hydrophones in the ocean. The recognition of a given signal is based on the relative distribution of its power among different frequency bands. The signal's power distribution is compared with a statistical model developed by analyzing relative power distributions of many signals of the same origin and a numerical criterion is calculated, which can serve as a measure of the probability for the signal to belong to the statistical model. Our recognition scheme was applied to 6-month-long continuous records of seven ocean bottom hydrophones (OBH) deployed in the Ligurian Sea. A maximum of 94% of all detectable teleseismic P-waves recorded during the deployment of the OBHs were recognized correctly with no false recognitions. The proposed recognition method will be implemented in autonomous underwater robots dedicated to detect and transmit acoustic signals generated by teleseismic P-waves. **Citation:** Sukhovich, A., J.-O. Irisson, F. J. Simons, A. Ogé, Y. Hello, A. Deschamps, and G. Nolet (2011), Automatic discrimination of underwater acoustic signals generated by teleseismic P-waves: A probabilistic approach, *Geophys. Res. Lett.*, *38*, L18605, doi:10.1029/2011GL048474.

1. Introduction

[2] Currently, there is a lack of seismic data collected over oceanic regions. The scarcity of seismic records from the oceans hampers the progress of global seismic tomography, especially when one attempts imaging of the southern hemisphere, which contains most of the known hot spots. The present approach to seismic data collection in the oceans includes the use of ocean bottom seismometers [*Webb*, 1998; *Stephen et al.*, 2003] and moored hydrophones [*Fox et al.*, 2001; *Dziak et al.*, 2004]. However, high installation and data recovery costs render these instruments too expensive to allow for a coverage that is sufficiently dense for the purposes of global seismic tomography. Teleseismic P-waves arriving at the ocean bottom are refracted into the water column and generate acoustic signals, which are of particular interest as their arrival times can be used in seismic tomography. *Simons et al.* [2009] have proposed to use autonomous freely-drifting underwater robots (called MERMAID, short for Mobile Earthquake Recording in Marine Areas by Independent Divers) equipped with hydrophones. By changing its buoyancy, the robot is able to dive to and remain at a certain depth. While at depth, the robot continuously monitors the pressure variation by calculating the ratio of short-term to long-term moving averages (STA/LTA algorithm) [*Allen*, 1978]. We wish that, once a strong teleseismic P-wave is detected, the robot immediately begins an ascent to establish satellite connection for the transmission of the recorded waveform. However, in oceanic domains there are many detectable acoustic signals generated by sources other than teleseismic earthquakes (e.g. ships, air gun campaigns, T-waves, marine animals). As each diving/re-surfacing cycle depletes the MERMAID's battery, it is of utmost importance to ensure that the robot surfaces only in case of a strong teleseismic P-wave detection. In this paper, we report on the development of a new probabilistic scheme that allows the automatic discrimination of teleseismic P-waves while missing very few of them and at the same time maintaining the probability of false recognitions at a minimum.

2. Method

[3] Our method begins with the analysis of a detected signal to obtain the distribution of its power among different frequency bands. This distribution is then compared to a statistical model for signals of a given type to calculate a numerical criterion, which can be regarded as a probability for the signal to be of this type. Based on the value of the criterion, the decision is taken on whether the MERMAID will or will not ascend.

[4] To obtain information on how the power of the signal is split among frequency bands, we use the discrete wavelet transform (DWT). Wavelet analysis has several advantages over conventional Fourier transforming of overlapping time windows. Just as the spectrogram, wavelet analysis provides information on both time behavior and frequency content of a signal. However, the DWT is non-redundant; it generates exactly as many wavelet coefficients as there are samples in the signal and thus requires fewer calculations. At the same time, simple and easy-to-program algorithms exist for calculating the DWT. In particular, we are using the "lifting" algorithm [*Sweldens*, 1996]. By removing small-magnitude, statistically unimportant wavelet coefficients, it is also possible to compress the signal and thus significantly reduce the amount of the data transmitted via satellite, as shown in the analysis by *Simons et al.* [2009]. Finally, the DWT can be performed in integer arithmetic with little or no loss of

[1]Géoazur, Villefranche-sur-Mer, France.
[2]Observatoire Océanologique, UPMC Université Paris 6, UMR 7093, LOV, Villefranche-sur-Mer, France.
[3]Observatoire Océanologique, CNRS, UMR 7093, LOV, Villefranche-sur-Mer, France.
[4]Department of Geosciences, Princeton University, Princeton, New Jersey, USA.
[5]Géoazur, Sophia Antipolis, France.

0094-8276/11/2011GL048474

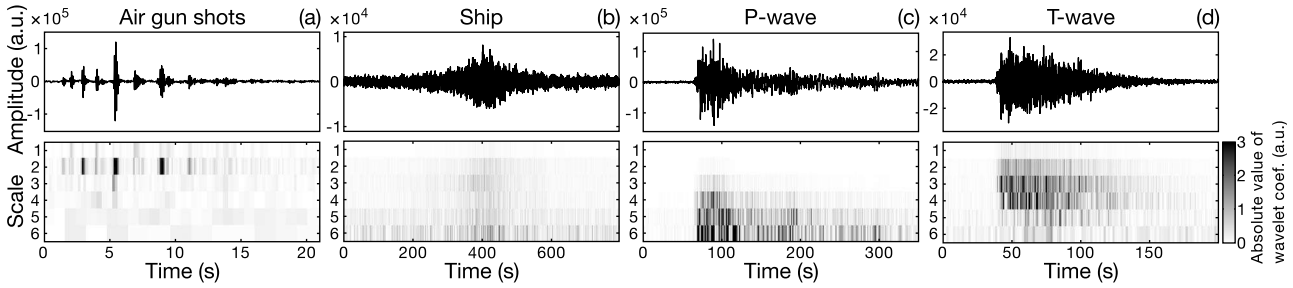

Figure 1. Representative acoustic signals generated by (a) an air gun, (b) a passing ship, (c) a teleseismic P-wave and (d) a T-wave with their scalograms. Each pixel in a scalogram represents the absolute value of a wavelet coefficient (arbitrary scale). The sampling rate of the signals is 40 Hz. The effective frequency range is thus between 0 and 20 Hz. The first scale of the DWT corresponds approximately to a passband covering the upper half of the original frequency range, 10–20 Hz; the second scale corresponds to 5–10 Hz, and so on. Note that most of the power of the teleseismic P-wave signal is at scales 5 and 6, which jointly cover the low frequency range between approximately 0.30 and 1.25 Hz, as expected.

accuracy, which helps to reduce the power consumption by the central processing unit. To improve accuracy of the integer DWT, we have modified the normalization part of the lifting algorithm, which originally involved division and multiplication by an irrational number. The details can be found in the auxiliary material.[1]

[5] In the wavelet transform analysis, the notion of frequency is replaced by the notion of a "scale". In a sense, the wavelet transformation is analogous to a filter-bank analysis, with overlapping filters covering different frequency bands [*Jensen and la Cour-Harbo*, 2001]. During wavelet transformation, every iteration produces a set of wavelet coefficients for each scale, which in its turn corresponds to a particular frequency band. As a rule of thumb, each subsequent scale has a passband centered around a frequency that is half of the center frequency of the previous scale. There exist many wavelet bases, among which the most suitable one can be chosen for the problem at hand. We use a biorthogonal wavelet basis with two and four vanishing moments for the primal and dual wavelets respectively, which is commonly abbreviated as CDF(2,4) [*Cohen et al.*, 1992]. As *McGuire et al.* [2008] found, this wavelet construction provides a very good compromise between computational effort and the filtering performance of the wavelets.

[6] The result of the wavelet analysis is most conveniently visualized by means of a scalogram, which presents the absolute values of the wavelet coefficients in the time-scale plane. The scalograms of representative signals of four different types analyzed in this paper are shown in Figure 1. We estimate the power of the detected signal at any scale by calculating the average of absolute values of its wavelet coefficients:

$$s_k = \frac{1}{N_k}\sum_{i=1}^{N_k}\left|w_i^k\right|, \tag{1}$$

where w_i^k is a wavelet coefficient, N_k is the number of the wavelet coefficients and indices i and k number time and scale, respectively. Strictly speaking, the estimate of the signal power should be done by calculating the average of the squares of wavelet coefficients; however, our definition is better suited for the calculations when the minimization of energy consumption is required. Equation (1) is evaluated for wavelet coefficients within a time window, whose limits are defined by the instances at which the STA/LTA ratio rises over 2 (trigger threshold) and then drops below 1 (de-trigger threshold). Note that after a trigger occurs, the LTA is still updated and thus affected by the triggering signal. By applying equation (1) to each scale, we obtain a set of scale averages s_k. To find the *relative* power distribution among the scales, the scale averages are normalized by their L_1 norm:

$$\tilde{s}_k = \frac{s_k}{L_1}, \quad \text{where } L_1 = \sum_{k=1}^{K} s_k. \tag{2}$$

[7] In our case the number of scales K equals 6. We subsequently divide each element $\tilde{s}_k$ by the corresponding element $\tilde{n}_k$ of the similar scale average calculated for the ambient noise record preceding the time of the STA/LTA trigger:

$$S_k = \frac{\tilde{s}_k}{\tilde{n}_k}. \tag{3}$$

[8] To better estimate the values of $\tilde{n}_k$, the scale averages are calculated for several overlapping noise records (512-samples-long taken with 10% overlap) and averaged to give a single element $\tilde{n}_k$ used in equation (3). This second normalization by ambient noise means that a pure noise record with no signal should give elements S_k with values close to 1 for all scales. For brevity, in the rest of the paper we will refer to the normalized scale averages S_k as simply "scale averages", while the term "normalized" should be implied.

[9] In order to derive statistical properties of signals of a certain origin, the scale averages S_k are calculated for as many pre-identified signals as possible and their distributions are obtained for each scale. We call this set of distributions the "statistical model" for the signals of this type (Figure 2). The recognition is performed by comparing the values of scale averages S_k^0 calculated for a detected signal with the statistical model for the signals generated by teleseismic P-waves. For each scale k, we compute the proportion p_k of the model scale averages S_k more extreme than S_k^0 (i.e. $S_k > S_k^0$ when S_k^0 lies to the right of the median and $S_k < S_k^0$ when S_k^0 lies to the left of the median); in other words, we estimate the area of the tail of the distribution beyond S_k^0. This is similar to quantifying the probability of committing an error known in statistics as a Type I error, which here means rejecting the signal as not belonging to

[1]Auxiliary materials are available in the HTML. doi:10.1029/2011GL048474.

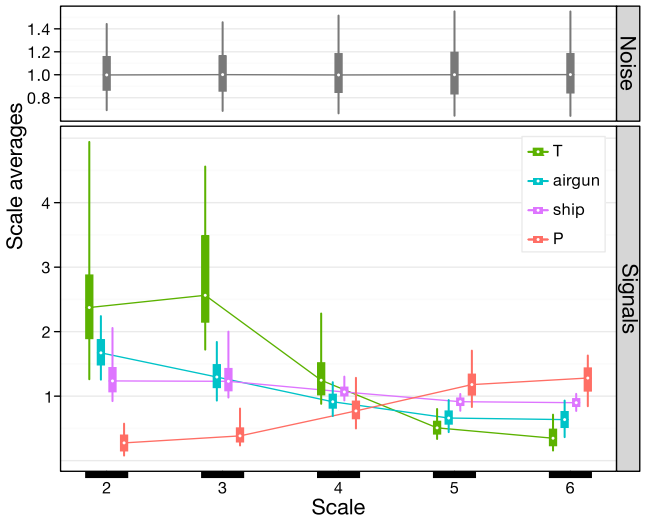

Figure 2. Description of the statistical models (top) for the ambient noise and (bottom) for the four types of signals recorded during the Grosmarin experiment. For each distribution of scale averages, the center point denotes the median, the box is delimited by the 25% and 75% quantiles and the vertical line ranges from the 5% to the 95% quantiles. The lines joining the medians of the distributions serve only as a guide for the eye.

the category of interest while it does. When S_k^0 is close to the median of the distribution, the probability of committing the Type I error is high since many S_k values are more extreme than S_k^0 and thus the computed proportion is high. We take the high probability of the Type I error as an indication that the detected signal is likely to be of the same origin as that of the signals used to create the statistical model. Conversely, when S_k^0 is located near one of the tails of the distribution, the probability of wrongly rejecting the signal is low. This serves as an indication that the signal is likely to be of a different origin.

[10] To combine the information from the various scales, multiplying the proportions would compute the probability to obtain a signal more extreme at *all* scales, which is too restrictive. Instead, we have found it to be much more effective to calculate a weighted average of p_k to obtain a single criterion C, ranging between 0 and 1 and quantifying the overall agreement between the detected signal and the statistical model:

$$C = \sum_k p_k D_k \Big/ \sum_k D_k, \tag{4}$$

where weights D_k are quantified by the Kolmogorov-Smirnov statistic [*Press et al.*, 1992]; more details on their calculation are given in the auxiliary material. When C is higher than a given threshold, we accept the signal as being a P-wave.

[11] The complement to the Type I error is the Type II error, i.e. the error of accepting the detected signal as belonging to the model while it does not. This error would cause the MERMAID to surface and transmit a signal generated by a source other than a teleseismic P-wave. We refer to such recognition as a "false positive". Minimizing or eliminating false positives is critically important for reducing the power consumption and thus for the overall success of the MERMAID's mission. We discuss our approach to ensure the absence of Type II errors after the presentation of our data analysis.

3. Data

[12] To determine the optimum threshold for C and to test the method, we have used continuous records of seven High Tech HTI-01-PCA hydrophones deployed at the bottom of the Ligurian Sea during the Grosmarin experiment, which was conducted between the end of April and the beginning of October 2008 [*Dessa et al.*, 2011]. The hydrophones were installed at distances ranging between 18 and 52 km from the coast and at depths ranging between 1300 and 2400 m within a square area of approximately 37.5 km × 50 km near (8.00E, 43.5N). The sampling rate was 100 Hz.

[13] To keep our analysis as close as possible to an actual mission of the MERMAID, the Grosmarin data were downsampled to 40 Hz after low-pass filtering with a numerical filter whose transfer function closely approximated the analogue 10 Hz low-pass filter installed on the MERMAID. Because of this low-pass filter, we did not consider the first scale of the wavelet transforms.

[14] The Grosmarin data set was very useful for the development of the method since it contains a large variety of noise signals detectable by the STA/LTA algorithm. First, cruise ships and ferries passed several times a day over the area of instruments' deployment. Also, the installation of the OBHs was followed by a continuous 3-day-long campaign of seismic shots using Bolt air guns which generated a large number of acoustic signals arriving at hydrophones from many angles and distances.

4. Results

[15] During the Grosmarin experiment, a total of 131 acoustic signals unambiguously generated by teleseismic P-waves were recorded and then used to produce a statistical model for teleseismic P-waves. These signals were identified by predicting the arrival times of the P-waves for known earthquakes. In addition, we have also created statistical models for three other types of signals which are most likely to be encountered by the MERMAID during an actual long-time mission: signals produced by air guns, passing ships and T-waves. The ship and T-wave signals were identified by eye. As explained in section 2, the scale averages for each signal were normalized by the scale averages of the preceding noise record. Therefore, the statistical model for the ambient noise was created as a reference model allowing us to validate the normalization by the ambient noise. This model was obtained by randomly choosing a large number of ambient noise record pairs (512-samples-long) from the full Grosmarin database and calculating normalized scale averages for each pair. All statistical models are shown in Figure 2.

[16] The statistical model describes how *on average* the power of the signals of a given origin is split among different scales (or equivalently, frequency bands). From Figure 2 it is already clear by eye that the power of the two types of geophysical interest (P- and T-waves) is distributed significantly differently from each other and from signals of other origins. The fact that ship signals are statistically close to the ambient noise may indicate a relatively high contribution of

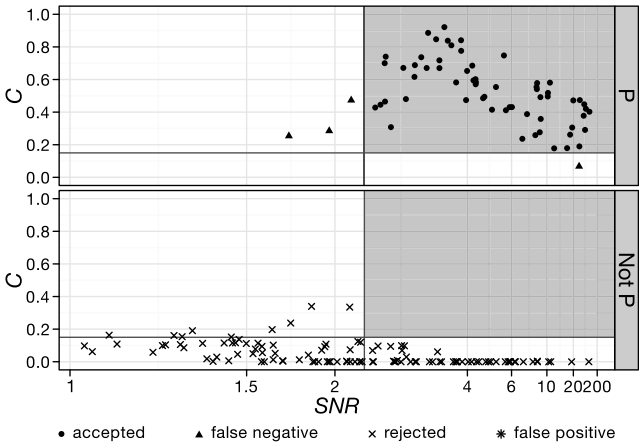

Figure 3. Positions of the signals, recorded during the Grosmarin experiment, in (*C*, *SNR*) space. Note that the *SNR* scale is not linear to better spread the points. Top panel shows teleseismic P-wave signals while the bottom panel shows all other signals. The figures allow visualization of the choice of thresholds for *C* and *SNR* in order to simultaneously maximize the number of correct recognitions and to minimize (or eliminate completely) the number of false positives. The shaded region on top and bottom figures is defined by the values of $C_0 = 0.15$ and $SNR_0 = 2.25$.

ships to the ambient noise. The inspection of the statistical model for teleseismic P-waves shows that most of the power is concentrated in scales 5 and 6, as expected for teleseismic events of large magnitude [*Aki*, 1967]. Also, all median values of the ambient noise model are very close to unity, as expected.

[17] After the recognition criterion *C* for a given signal is obtained, we must decide which numerical value should be taken as an indicator of a teleseismic P-wave detection with high probability. To this end, we simulated the MERMAID's mission by running the STA/LTA algorithm on the full Grosmarin database and calculated *C* for each detected signal using the P-wave statistical model. In addition to *C*, we calculated signal-to-noise ratio (SNR) values defined as:

$$SNR = \sum_{k=2}^{K} s_k \Big/ \sum_{k=2}^{K} n_k, \tag{5}$$

where s_k and n_k are given by equation (1). A total of 176 signals were detected by the STA/LTA algorithm. Figure 3 shows the detected signals according to their *C* and *SNR* values. It is evident that most of the signals of non-P-wave origin (lower panel of Figure 3) with high value of *C* have low values of *SNR*. At the same time, the non-P-wave signals with high *SNR* have very low values of *C*. Therefore, by choosing thresholds for both *C* and *SNR*, we can eliminate false positive recognitions. With thresholds $C_0 = 0.15$ and $SNR_0 = 2.25$, 94% (61 out of 65) of detected P-wave signals are recognized correctly with no false positives. Even with more conservative thresholds $C_0 = 0.2$ and $SNR_0 = 3.1$, which would further limit the possibility of false positive recognitions, the recognition rate of P-wave signals was still 69%. Although there is no guarantee that false positives will be completely eliminated in a future independent data set, the choice of C_0 and SNR_0 is obviously a good one. In MERMAID deployments we plan to use the most conservative thresholds to decide if the robot should surface immediately upon a teleseismic P-wave detection, while using *C* to rank less certain detections by their priority in a (finite) buffer for transmission at the next surfacing. The exact values of the thresholds are yet to be determined; in fact, we are still in the process of collecting noise data before committing ourselves to a fixed strategy. The lateral drift during an ascent of about 2.5 hours depends on the local oceanic currents and is at most a few hundred meters so that the GPS location upon surfacing should be accurate enough for seismic tomography. The geolocation of the stored events will require interpolation [e.g., *Taillandier et al.*, 2006]. To keep interpolation errors acceptable, the robot will surface at least every 10–15 days, depending on location.

[18] All detected signals with high *SNR* (>5) but not originating from teleseismic P-waves (Figure 3, bottom), are ruled out even with a very moderate threshold $C_0 = 0.1$. We found that most of these strong signals were T-waves. The T-waves are expected to be frequently detected by the MERMAIDs whose programmed parking depth (around 1500 m) at low- and mid-latitudes will be within the depth range of the axis of the Sound Fixing And Ranging channel, where T-waves propagate over long distances with very little attenuation [*Dziak et al.*, 2004]. Since T-waves are unsuitable for seismic tomography, it is very important that our method is able to eliminate them with high efficiency.

[19] As a final test, we have applied the recognition method to an independent data set obtained with the same instrument as in the Grosmarin experiment, but deployed near the coast of Haiti (72.97W, 18.62N) at the depth of 1508 m during a 4-month-long period after the devastating earthquake in January 2010. By using the statistical model for P-waves obtained from the Grosmarin data and the thresholds $C_0 = 0.15$ and $SNR_0 = 2.25$ we recognized 75% (21 out of 28) of teleseismic P-wave signals with only two false positives. One of these false positives was produced by a high-amplitude spike signal due to electronic noise. The other much weaker signal, although closely resembling a P-wave, was tentatively classified as a false positive since we were not able to identify its source earthquake. The application of more conservative thresholds $C_0 = 0.2$ and $SNR_0 = 3.1$ resulted in 46% of correct recognitions while ruling out the tentative false positive.

[20] The statistical models presented in this paper were developed from the data recorded by instruments used during the Grosmarin experiment. One would expect that the normalization by a preceding ambient noise record will render the method insensitive to instrument response. However, a wavelet decomposition is not equivalent to a Fourier transform, and one can show that the instrument response does not divide out perfectly during the normalization. In addition, care should be taken not to include scales that are mostly outside the passband of the instrument. Finally, the noise characteristics may be different depending on geographical location. We therefore recommend not to blindly adopt the criteria developed in this paper (although they may provide a good starting point in most cases), but to perform an analysis separately for each pool of equivalent instruments and for each geographical location, if possible.

[21] It seems worthwhile comparing our recognition scheme with other existing methods applicable to an auto-

matic recognition of teleseismic events. Similar to our method, all of them analyze both time and frequency properties of seismograms. *Evans and Allen* [1983] use two STA/LTA ratios calculated simultaneously for high-passed and low-passed versions of a seismogram, and call an event detected when triggering for the low-passed version but not for the high-passed one. *Goforth and Herrin* [1981] compute coefficients of the Walsh transform (which in a broad sense is analogous to Fourier transform) of overlapping time windows. The distribution of the absolute values of the coefficients corresponding to the frequency band of interest is obtained and detection is declared when the similar sum for subsequent time windows falls out of a pre-set confidence interval. *Gledhill* [1985] uses the Discrete Fourier Transform on a 10-s-long time window to estimate spectral power within five equal frequency bands and compares band levels with average band levels obtained from similar analysis on preceding 512 time windows. The above methods are similar in that they all use negative decision logic, i.e. the detection is declared based on the detected deviations from the ambient noise. Our approach is different as we test for positive correlation between a signal and a given statistical model. In this sense, our method is similar to the one by *Joswig* [1990], whose recognition algorithm tests the degree of correlation between a continuously updated pattern of a seismogram and patterns corresponding to the signals of known origins. However, his patterns (two-dimensional gray scale pictures) are calculated from scaled spectrograms whose calculation involves significantly larger amount of computations as compared to the DWT [*Simons et al.*, 2009]. Our method thus seems to be better suited for platforms with limited power supply such as MERMAIDs. Finally, to the best of our knowledge, our method is the first one which utilizes the probabilistic approach and allows to estimate the probability of false positive recognitions.

[22] Note that our method is not limited to the recognition of teleseismic P-waves. Provided the statistical model of the signals whose automatic recognition is sought is sufficiently different from those of the signals of other types (most likely to be encountered by a detecting instrument) the proposed recognition method should work. In particular, the method seems to be readily applicable to the automatic recognition of T-waves (Figure 2).

5. Conclusions

[23] We have presented a new method for the automatic recognition of underwater acoustic signals generated by teleseismic P-waves. The method is based on the analysis of the relative power distribution among different frequency bands and utilizes the DWT as a signal processing tool. By analyzing the relative power distributions of a large number of P-wave signals, we derived a statistical model for P-waves. The resemblance between a detected signal and the statistical model is quantified by the criterion C, which is akin to a probability of committing the Type I error during recognition (i.e. rejecting a P-wave signal while it should be accepted). It was also shown that the SNR of the analyzed signal can be used as an additional recognition criterion and can help eliminate false positive recognitions. Our method is not limited to the recognition of teleseismic P-waves and can be applied to the recognition of any signals whose statistical models differ sufficiently from those of other intervening signals.

[24] **Acknowledgments.** We wish to thank J. Perrot for helpful discussions on T-waves. This work was supported by European Research Council (Advanced grant 226837) and by Marie Curie Re-integration grant (project 223799).

[25] The Editor thanks the two anonymous reviewers for their assistance in evaluating this paper.

References

Aki, K. (1967), Scaling law of seismic spectrum, *J. Geophys. Res.*, *72*(4), 1217–1231.

Allen, R. V. (1978), Automatic earthquake recognition and timing from single traces, *Bull. Seismol. Soc. Am.*, *68*(5), 1521–1532.

Cohen, A., I. Daubechies, and J. Feauveau (1992), Biorthogonal bases of compactly supported wavelets, *Commun. Pure Appl. Math.*, *45*, 485–560.

Dessa, J.-X., S. Simon, M. Lelièvre, M.-O. Beslier, A. Deschamps, N. Béthoux, S. Solarino, F. Sage, E. Eva, G. Ferretti et al. (2011), The GROSMarin experiment: three dimensional crustal structure of the North Ligurian margin from refraction tomography and preliminary analysis of microseismic measurements, *Bull. Soc. Geol. Fr.*, *182*(4), 305–321.

Dziak, R. P., D. R. Bohnenstiehl, H. Matsumoto, C. G. Fox, D. K. Smith, M. Tolstoy, T.-K. Lau, J. H. Haxel, and M. J. Fowler (2004), *P*- and *T*-wave detection thresholds, *Pn* velocity estimate, and detection of lower mantle and core *P*-waves on ocean sound-channel hydrophones at the Mid-Atlantic Ridge, *Bull. Seismol. Soc. Am.*, *94*(2), 665–677.

Evans, J., and S. S. Allen (1983), A teleseism-specific detection algorithm for single short period traces, *Bull. Seismol. Soc. Am.*, *73*(4), 1173–1186.

Fox, C. G., H. Matsumoto, and T.-K. A. Lau (2001), Monitoring Pacific Ocean seismicity from an autonomous hydrophone array, *J. Geophys. Res.*, *106*(B3), 1347–1352.

Gledhill, K. R. (1985), An earthquake detector employing frequency domain techniques, *Bull. Seismol. Soc. Am.*, *75*(6), 1827–1835.

Goforth, T., and E. Herrin (1981), An automatic seismic signal detection algorithm based on the Walsh transform, *Bull. Seismol. Soc. Am.*, *71*(4), 1351–1360.

Jensen, A., and A. la Cour-Harbo (2001), *Ripples in Mathematics*, Springer, Berlin.

Joswig, M. (1990), Pattern recognition for earthquake detection, *Bull. Seismol. Soc. Am.*, *80*(1), 170–186.

McGuire, J. J., F. J. Simons, and J. A. Collins (2008), Analysis of seafloor seismograms of the 2003 Tokachi-Oki earthquake sequence for earthquake early warning, *Geophys. Res. Lett.*, *35*, L14310, doi:10.1029/2008GL033986.

Press, W., S. Teukolsky, W. Vettering, and B. Flannery (1992), *Numerical Recipes*, 2nd ed., Cambridge Univ. Press, Cambridge, U. K.

Simons, F. J., G. Nolet, P. Georgief, J. M. Babcock, L. A. Regier, and R. E. Davis (2009), On the potential of recording earthquakes for global seismic tomography by low-cost autonomous instruments in the oceans, *J. Geophys. Res.*, *114*, B05307, doi:10.1029/2008JB006088.

Stephen, R. A., F. N. Spiess, J. A. Collins, J. A. Hildebrand, J. A. Orcutt, K. R. Peal, F. L. Vernon, and F. B. Wooding (2003), Ocean seismic network pilot experiment, *Geochem. Geophys. Geosyst.*, *4*(10), 1092, doi:10.1029/2002GC000485.

Sweldens, W. (1996), The lifting scheme: A custom-design construction of biorthogonal wavelets, *Appl. Comput. Harmonic Anal.*, *3*(2), 186–200.

Taillandier, V., A. Griffa, P.-M. Poulain, and K. Béranger (2006), Assimilation of Argo float positions in the north western Mediterranean Sea and impact on ocean circulation simulations, *Geophys. Res. Lett.*, *33*, L11604, doi:10.1029/2005GL025552.

Webb, S. C. (1998), Broadband seismology and noise under the ocean, *Rev. Geophys.*, *36*(1), 105–142.

A. Deschamps and G. Nolet, Géoazur, 250, Rue Albert Einstein, F-06560 Sophia Antipolis, France.

Y. Hello, A. Ogé, and A. Sukhovich, Géoazur, Observatoire Océanologique de Villefranche-sur-Mer, 2 quai de la Darse, BP 48, F-06235 Villefranche-sur-Mer, France. (alexey.sukhovich@geoazur.obs-vlfr.fr)

J.-O. Irisson, Observatoire Océanologique, Station Zoologique, BP 28, Chemin du Lazaret, F-06230 Villefranche-sur-Mer, France.

F. J. Simons, Department of Geosciences, Princeton University, Guyot Hall 321B, Princeton, NJ 08544, USA.

Auxiliary material for paper 2011GL048474

Title:

Automatic discrimination of underwater acoustic signals generated by teleseismic P-waves: A probabilistic approach

Modified normalization of the lifting algorithm for calculation of an integer discrete wavelet transform (DWT)

We present an algorithm for the forward CDF(2,4) wavelet transform which is optimized for an integer arithmetic and based on the lifting scheme [*Sweldens*, 1996]. An application of the lifting scheme to a signal of length of a power of two, transforms the signal into a pair of vectors a and d, each twice as short as the original signal. Vector d, sometimes called "details", contains wavelet coefficients for a corresponding wavelet transform scale. Vector a, sometimes called "approximations", contains scaling coefficients and is used as an input for the next application of the lifting scheme, which produces new vectors a and d, with d containing wavelet coefficients for the next scale, and so on. To avoid numerical divergence of the wavelet transform, newly calculated vectors a and d are normalized by multiplying and dividing by $\sqrt{2}$ correspondingly. These two numerical factors, being irrational numbers, can be approximated in integer arithmetic by a ratio of two integer numbers. To multiply or divide by $\sqrt{2}$, one would multiply or divide by numerator and then divide or multiply by the denominator of the ratio correspondingly. This approximation however degrades the precision of the calculations. The normalization by two irrational numbers can be partially avoided, if one notes that:

1. The lifting scheme is linear.
2. Multiplication by $\sqrt{2}$ of the vector a_i obtained after calculation of an odd scale ($i = 1, 3, 5, ...$), is canceled by dividing vector d_{i+1}, obtained after the calculation of the next (even) scale, by $\sqrt{2}$. In other words, vector d_{i+1} is the same whether the input vector a_i was or was not normalized.
3. At the same time, multiplication of vector a_{i+1} by $\sqrt{2}$ produces the same result as multiplication by an integer number 2 in case when the input vector a_i was not normalized.

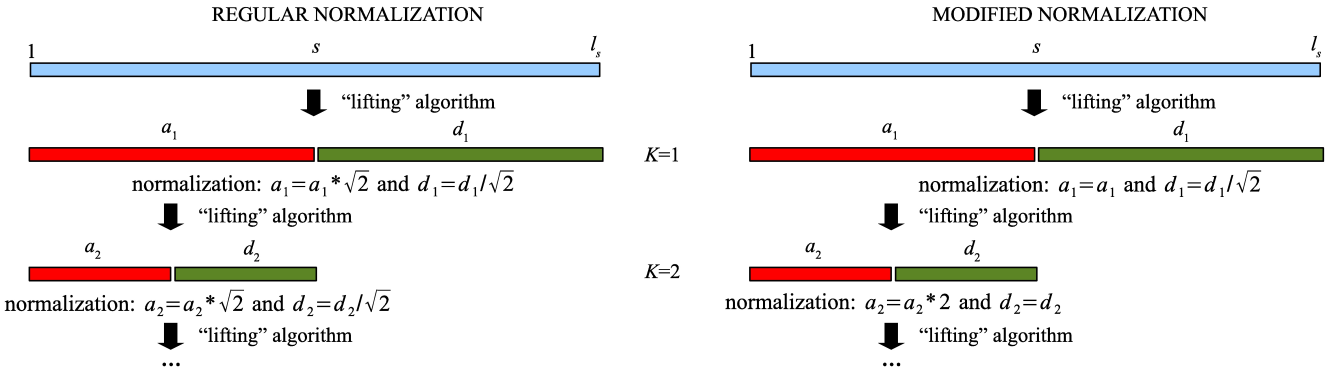

Figure S1: Comparison of two ways to perform the normalization during calculation of the DWT with lifting algorithm. With the modified normalization, three out of four operations with $\sqrt{2}$ are removed. K is a scale number, l_s is a number of samples in vector s.

We take advantage of the above properties of the lifting scheme to reduce the number of normalization operations with $\sqrt{2}$. In our modified algorithm, each odd vector a_i ($i = 1, 3, 5, ...$) is not normalized, and each even vector a_{i+1} is normalized by multiplying by 2. At the same time, odd vectors d_i are divided by $\sqrt{2}$, while vectors d_{i+1} are left unchanged (Figure S1).

The following Matlab code shows the implementation of our modified algorithm for calculation of a K-scale CDF(2,4) wavelet transform (see also *Simons et al.* [2006] for comparison):

```
ls = length(s);

for j = 1:K;
    for n = 2:2:ls–2
        s(n) = s(n) – [s(n–1) + s(n+1)]/2;
    end

    for n = 5:2:ls–3
        s(n) = s(n) – 3*[s(n–3) + s(n+3)]/64 + 19*[s(n–1)+s(n+1)]/64;
    end

    d = s(2:2:ls);
    a = s(1:2:ls);

    % normalization part
    if (mod(j,2) == 1)
        % odd scale
        d = d/sqrt(2);
    else
        % even scale
        a = a*2;
    end

    s(1:ls/2) = a;
    s(ls/2 + 1:ls) = d;

    ls = length(s)/2^j;

end
```

In this code, an input signal s is transformed into the same-length vector s, which contains scaling and wavelet coefficients arranged in a Mallat multi-resolution ordering [*Mallat*, 1998]. For simplicity, no treatment of the boundary points $s(1), s(3), s(ls-1), s(ls)$, where ls is the length of the vector s, is performed; however, in the actual code we introduce edge corrections by treating boundary points with lower order wavelet transforms: CDF(1,1) (also known as Haar transform) and CDF(2,2). Interested readers will find the details on the treatment of the boundary effects in *Jensen and la Cour-Harbo* [2001].

Calculation of the scale weights D_k

Figure S2 shows the histograms of the scale averages for the signals generated by P-waves and for all other types of signals combined (air guns, ships and T-waves). While there is little difference between P-wave signals and signals of other origins at scale 4, the difference at remaining scales can be substantial (e.g. virtually no overlap at scale 2). To take advantage of these differences, the criterion C is computed by weighting each proportion p_k of extreme scale averages by the corresponding weight D_k (Equation (4) of the manuscript). For each scale k, the weight is obtained by calculating the Kolmogorov-Smirnov statistic D [*Zar*, 1999; *Press et al.*, 1992] between each pair of distributions shown in Figure S2. Essentially, weights D_k represent the differentiating powers of the corresponding scales during the process of discrimination.

The values of D_k are indicated in Figure S2. It also shows that the distributions of scale averages for

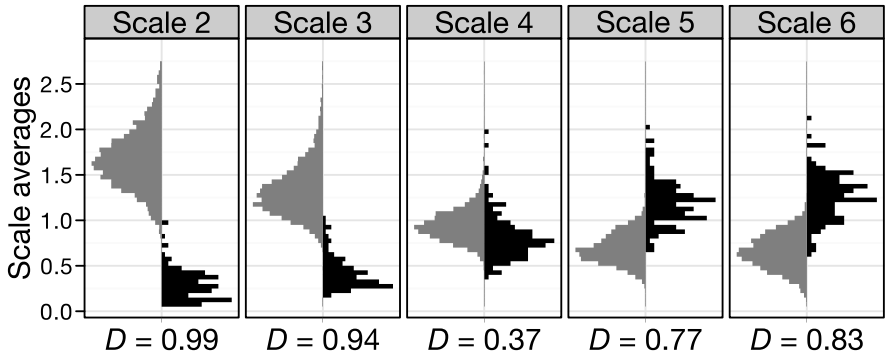

Figure S2: Back-to-back histograms showing the normalized distributions (highest bar scaled to 1) of the scale averages of teleseismic P-waves (black, right side) and all other signals (air guns, ships, and T-waves; gray, left side) at scales 2–6. A total of 131 P-wave signals and 3880 signals of other origins were used to produce the histograms. At each scale, the two distributions are compared using the Kolmogorov-Smirnov method and the value of the statistic D is reported. D varies between 0 (perfect match) and 1 (complete mismatch).

the P-wave model are not symmetric. A maximum-likelihood fit and another Kolmogorov-Smirnov test has shown that the distributions are not significantly different from a log-normal distribution. This was found to be true for most models' distributions (except for those at scale 6 of ambient noise and air gun signal models and scales 2, 3, and 4 of ship signal model).

References

Jensen, A., and A. la Cour-Harbo (2001), *Ripples in Mathematics*, Springer, Berlin.

Mallat, S. (1998), *A Wavelet Tour of Signal Processing*, Academic Press, San Diego.

Press, W., S. Teukolsky, W. Vettering, and B. Flannery (1992), *Numerical Recipes*, second ed., Cambridge University Press, Cambridge, UK.

Simons, F. J., B. D. E. Dando, and R. M. Allen (2006), Automatic detection and rapid determination of earthquake magnitude by wavelet multiscale analysis of the primary arrival, *Earth and Planetary Science Letters*, *250*, 214–223, doi:10.1016/j.epsl.2006.07.039.

Sweldens, W. (1996), The lifting scheme: A custom-design construction of biorthogonal wavelets, *Appl. Comput. Harmon. Anal.*, *3*(2), 186–200.

Zar, J. H. (1999), *Biostatistical analysis*, 4th ed., Prentice Hall, New Jersey.